Journal of Innate Immunity

Research Article

J Innate Immun 2023;15:37–49
DOI: 10.1159/000524693

Received: December 20, 2021
Accepted: March 16, 2022
Published online: June 7, 2022

Mannan-Binding Lectin Reduces Epithelial-Mesenchymal Transition in Pulmonary Fibrosis via Inactivating the Store-Operated Calcium Entry Machinery

Yunzhi Liu[a, b] Xianghuan Xie[b] Ping Wang[b] Jialiang Luo[a, b] Yu Chen[a, b] Qishan Xu[c] Jia Zhou[b] Xiao Lu[b] Jianbo Zhao[d] Zhengliang Chen[b] Daming Zuo[a, c]

[a]Department of Medical Laboratory, School of Laboratory Medicine and Biotechnology, Southern Medical University, Guangzhou, China; [b]Guangdong Province Key Laboratory of Proteomics, Department of Immunology, School of Basic Medical Sciences, Southern Medical University, Guangzhou, China; [c] Microbiome Medicine Center, Zhujiang Hospital, Southern Medical University, Guangzhou, China; [d]Division of Vascular and Interventional Radiology, Department of General Surgery, Nanfang Hospital, Southern Medical University, Guangzhou, China

Keywords
Idiopathic pulmonary fibrosis · Mannan-binding lectin · Epithelial-mesenchymal transition · Store-operated calcium entry · PDK1

Abstract
Idiopathic pulmonary fibrosis (IPF) is a type of idiopathic interstitial pneumonia with a poor clinical prognosis. Increasing evidence has demonstrated that epithelial-mesenchymal transition (EMT) contributes to the production of pathogenic myofibroblasts and plays a pivotal role in the development of pulmonary fibrosis. Mannan-binding lectin (MBL) is a soluble calcium-dependent complement molecule. Several studies have reported associations between serum MBL levels and lung diseases; however, the effect of MBL on IPF remains unknown. The present study observed aggravated pulmonary fibrosis in bleomycin-treated $MBL^{-/-}$ mice compared with their wild-type counterparts. Lung tissues from bleomycin-treated $MBL^{-/-}$ mice displayed a more severe EMT phenotype. In vitro studies determined that MBL inhibited the EMT process through attenuating store-operated calcium entry (SOCE) signaling. It was further demonstrated that MBL promoted the ubiquitination of Orai1, an essential component of SOCE, via pyruvate dehydrogenase kinase 1 (PDK1)-serum glucocorticoid-regulated kinase 1 signaling. PDK1 inhibition abolished the MBL-mediated regulation of SOCE activity and the EMT process. Notably, biochemical analysis showed that MBL interacted with PDK1 and contributed to PDK1 ubiquitination. In summary, the present findings suggested that MBL limited the EMT phenotype in human alveolar epithelial cells through regulation of SOCE, and MBL could be recognized as a potential therapeutic target for IPF.

Introduction

Idiopathic pulmonary fibrosis (IPF) is a type of idiopathic interstitial pneumonia, which commonly develops with progressive pulmonary scarring and abnormal ex-

Karger@karger.com
www.karger.com/jin

Correspondence to:
Jianbo Zhao, zhaojianbohgl@163.com
Zhengliang Chen, zhlchen@smu.edu.cn
Daming Zuo, zdaming@smu.edu.cn

tracellular matrix production. IPF affects ~50,000 patients annually in Asia and South America, and the clinical prognosis for patients with IPF remains poor [1]. Alveolar epithelial type II cells are the heterogeneous progenitors in lung tissues since they maintain the alveolar epithelium through self-renewal and differentiation into alveolar epithelial type I cells for tissue repair [2]. Dysfunction of the alveolar epithelium to regenerate after damage was considered to be the most reliable hypothesis for IPF development [3]. Epithelial-mesenchymal transition (EMT) is a dynamic process in which epithelial cells abolish the expression of epithelial proteins and acquire a mesenchymal phenotype [4]. Notably, pulmonary fibrosis is a type II EMT event, in which the process physiologically occurs in response to injury, and terminates when tissue repair results in wound healing and subsequent regeneration [5]. Increasing evidence has showed that, during pulmonary fibrogenesis, EMT is a significant source of pathogenic myofibroblasts. Indeed, EMT has been detected in lung tissue from patients with IPF and animal models of pulmonary fibrosis [6, 7]. EMT has been reported to be a pivotal event in the development of pulmonary fibrosis. Induction of EMT-like phenotypes of lung epithelial cells markedly exacerbated the process of pulmonary fibrosis in mice [8]. TGF-β is considered to be a significant inducer of EMT, which exerts a crucial effect on the pathogenesis of IPF by promoting the fibrotic process [9]. Thus, it is critical to investigate the modulation of the EMT process along with the course of pulmonary fibrosis.

Mannan-binding lectin (MBL) belongs to the C-type lectin family and is primarily synthesized in the liver and then released into the blood [10, 11]. MBL recognizes a variety of pathogenic microorganisms, leading to the initiation of the complement cascade through the lectin pathway. Several clinical studies have reported that individuals with MBL deficiency are predisposed to severe respiratory tract infection [12]. Mandal et al. [13] observed that a specific MBL haplotype was associated with frequent exacerbations of chronic obstructive pulmonary disease, and high serum MBL levels were associated with increased survival in a longitudinal study. Paradoxically, a previous study showed that MBL deficiency in chronic obstructive pulmonary disease limited the risk of aggravations and was associated with a more diverse lung microbiota [13]. Notably, MBL has been suggested to act as a supplement to cure smoking-related lung inflammation in a murine study [14]. However, activating the MBL pathway resulted in a worse outcome in patients with SARS-CoV-2 infection [15]. Although MBL has been studied on lung diseases, the effect of MBL on IPF remains unknown.

Bleomycin (BLM)-induced pulmonary fibrosis is the most well-characterized experimental study model of human IPF [16]. Delivery of BLM to the lung directly damages alveolar epithelial cells (AECs) and induces rapidly developing fibrosis after a single administration. In the present study, MBL-deficient ($MBL^{-/-}$) mice were employed to investigate the potential effect of MBL on BLM-induced pulmonary fibrosis. The results showed that MBL deficiency facilitated the EMT process in the lung and aggravated BLM-induced pulmonary fibrosis. MBL regulated the level of store-operated calcium entry (SOCE) in the lung epithelium in response to TGF-β stimulation. Furthermore, it was demonstrated that MBL regulated the processes of SOCE and EMT through interacting with pyruvate dehydrogenase kinase 1 (PDK1). In summary, the present findings suggested a new function for MBL in the EMT process, which offers insight into lung pathophysiology in patients with MBL deficiency and provides novel opportunities to develop future therapeutic strategies for fibrotic disease.

Materials and Methods

Animals

Wild-type (WT) C57BL/6J mice were purchased from the Laboratory Animal Center of Southern Medical University (Guangzhou, China). MBL-deficient ($MBL^{-/-}$) mice were purchased from the Jackson Laboratory (strain: 129S4/SvJae). Mice were housed under a 12-h light/dark cycle condition at a constant temperature (19–23°C) and (55 ± 10%) humidity, had free access to water and a commercial diet. All animal experiments in this study were approved by the Welfare and Ethical Committee for Experimental Animal Care of Southern Medical University (Approval number: L2016014). All mice were euthanized with 5% isoflurane.

BLM-Induced IPF Model

Five milligrams per kilogram BLM (9041-93-4; Aladdin, Inc.) or equal amounts of PBS were intratracheally injected into 8-week-old male WT or $MBL^{-/-}$ mice as previously described [17]. In some cases, mice were injected combined with 10-mg/kg BTP2 (S8380; Selleck). Mice were sacrificed 21 days after BLM administration. Lung tissues were lavaged three times with 0.5-mL PBS for bronchoalveolar lavage fluid (BALF) collection. BALF was centrifugated at 450 *g* for 5 min at 4°C. Then, the supernatant was kept for total protein measurement, and the precipitants were collected for cell count detection. Cell count detection was performed manually using an improved Neubauer hemocytometer.

To determine differential cell count, slides were prepared by cytospin centrifuge at 500 rpm for 5 min. Slides were prepared at a concentration of $50–70 \times 10^3$ cells per slide and then stained with diff-quick staining.

Table 1. Primers for the target genes

Gene	Forward primer (5'→3')	Reverse primer (5'→3')
(m)E-cadherin	CAGGTCTCCTCATGGCTTTGC	CTTCCGAAAAGAAGGCTGTCC
(m)N-cadherin	ATAGCCCGGTTTCACTTGAGA	CAGGCTTTGATCCCTCTGGA
(m)Vimentin	CTGCTTCAAGACTCGGTGGAC	ATCTCCTCCTCGTACAGGTCG
(m)α-SMA	TCAGGGAGTAATGGTTGGAATG	CCAGAGTCCAGCACAATACCAG
(m)GAPDH	CCTCGTCCCGTAGACAAAATG	TGAGGTCAATGAAGGGGTCGT
(h)E-cadherin	CATTTCCCAACTCCTCTCCTGGC	ATGGGCCTTTTTCATTTTCTGGG
(h)N-cadherin	CCACGCCGAGCCCCAGTATC	CCCCCAGTCGTTCAGGTAATCA
(h)Vimentin	GACGCCATCAACACCGAGTT	CTTTGTCGTTGGTTAGCTGGT
(h)α-SMA	AGAAGCCCAGCCAGTCGCCATCA	AGCAAAGCCCGCCTTACAGAGCC
(h)Orai1	GACTGGATCGGCCAGAGTTAC	GTCCGGCTGGAGGCTTTAAG
(h)Stim1	AGTCACAGTGAGAAGGCGAC	CAATTCGGCAAAACTCTGCTG
(h)GAPDH	CATCACTGCCACCCAGAAGACTG	ATGCCAGTGAGCTTCCCGTTCAG

Histological Analysis

The hydroxyproline level was determined by a hydroxyproline detection kit (MAK008-1KT; Sigma-Aldrich). Lung tissues were isolated and fixed with 4% paraformaldehyde. The sections were performed with hematoxylin and eosin (H&E) staining for pathological analysis. The Masson trichrome staining was evaluated using a commercial kit (G1346; Solarbio) following the manufacturer's protocol.

Cell Culture and Treatment

The human bronchial epithelial (HBE) cells were cultured in DMEM medium (11965092; Thermo Fisher Scientific, Inc) supplemented with 10% fetal bovine serum, 100-U/mL penicillin, and 100-μg/mL streptomycin at 37°C in 5% CO_2. To induce the EMT process in vitro, HBE cells were cultured in a serum-free medium and stimulated with 10-ng/mL TGF-β for 24 h. MBL protein was prepared as previously described [18]. In some cases, cells were treated combined with 10-μg/mL MBL, 3-μM BTP2, 10-μM MG132 (S2619; Selleck), or 5-μM GSK2334470 (S7087; Selleck).

RT-qPCR Analysis

Lung tissues or HBE cells were added in 1-mL TRIzol® (Thermo Fisher Scientific, Inc.), and total RNA was extracted based on TRIzol method. Then, 1,000-ng RNA was synthesized into cDNA in 50°C for 10 min and 85°C for 5-s conditions. SYBR Green Real-Time PCR Master Mix (A46112; Applied Biosystems; Thermo Fisher Scientific, Inc.) was applied for qPCR on an ABI Prism 7500 Sequence Detection System (Applied Biosystems; Thermo Fisher Scientific, Inc.), according to the following conditions: initial denaturation at 94°C for 30 s, followed by 40 cycles of denaturation at 94°C for 5 s, extension at 60°C for 30 s. The expression of the target genes was normalized to GAPDH gene expression and determined using the $2^{-\Delta\Delta Ct}$ method. The primer sequences involved in this experiment are shown in Table 1.

Wound Healing Assay

HBE cells were scratched using a sterile 1-mL pipette tip. The cells were cultured without fetal bovine serum and treated with 10-ng/mL TGF-β in the presence or absence of 10-μg/mL MBL or 3-μM BTP2 for 24 h. The distance between the wound edges was measured using Image J software.

Measurements of Cytoplasmic Ca^{2+} Concentration

Cal-520 AM was purchased from AAT Bioquest (20650) and dissolved in DMSO as a transitional solvent. Cultured cells were washed three times with DMEM medium and stained with 1-μM Cal-520 AM at 37°C for 60 min. Then they were washed three times using D-Hanks buffer. The cellular calcium levels in cells were detected by FACS LSRFortessa™. For SOCE detection, 1 μM thapsigargin (TG) was added to deplete internal calcium stores. The Ca^{2+} influx was induced by adding 1 mM $CaCl_2$ post-store depletion. Fluorescence imaging was carried out at the excitation and emission wavelengths of 488 nm and 526 nm, respectively, using a confocal laser scanning microscope (LSM 880 with Airyscan; Zeiss). The cellular Ca^{2+} levels are presented as a ratio of F/F0. F0 indicated the baseline fluorescence intensity detected after TGF-β treatment, and F was the fluorescence intensity measured at indicated time points.

Immunoprecipitation and Western Blot

Whole-cell lysates were incubated with 1 μg antibodies at 4°C overnight and treated with protein A/G agarose (Santa Cruz Biotechnology) for another 2 h at 4°C. The eluted immunoprecipitants were assayed by SDS-PAGE. For ubiquitination assay, HBE cells were pretreated with 10 μM MG132 for 4 h before collecting cells for immunoprecipitation. For western blot analysis, protein samples were separated on SDS-PAGE and then transferred onto polyvinylidene fluoride membranes. After blocking with 5% BSA for 1 h at room temperature, the membranes were incubated with indicated primary antibodies at 4°C overnight. The membranes were then stained with HRP-conjugated secondary antibody (S0001; Affinity Biosciences) at room temperature for another 1 h. Antibodies involved in this subsection are listed below: E-cadherin (14472, mouse anti-human monoclonal antibody, 1:1,000 dilution; Cell Signaling Technology), N-cadherin (22018-1-AP, rabbit anti-human polyclonal antibody, 1:1,000 dilution; Proteintech), α-SMA (14395-1-AP, rabbit anti-human polyclonal antibody, 1:1,000 dilution; Proteintech), vimentin (10366-1-AP, rabbit anti-human polyclonal antibody, 1:1,000 dilution; Proteintech), Orai1 (66223-1-Ig, rabbit anti-human polyclonal antibody, 1:1,000 dilution; Proteintech), Stim1 (5668, rabbit anti-human monoclonal antibody, 1:1,000 dilution; Cell Signaling Technology), SGK1 (23394-1-AP, rabbit anti-human polyclonal antibody, 1:1,000 dilution; Proteintech), PDK1 (17086-1-AP, rabbit anti-human poly-

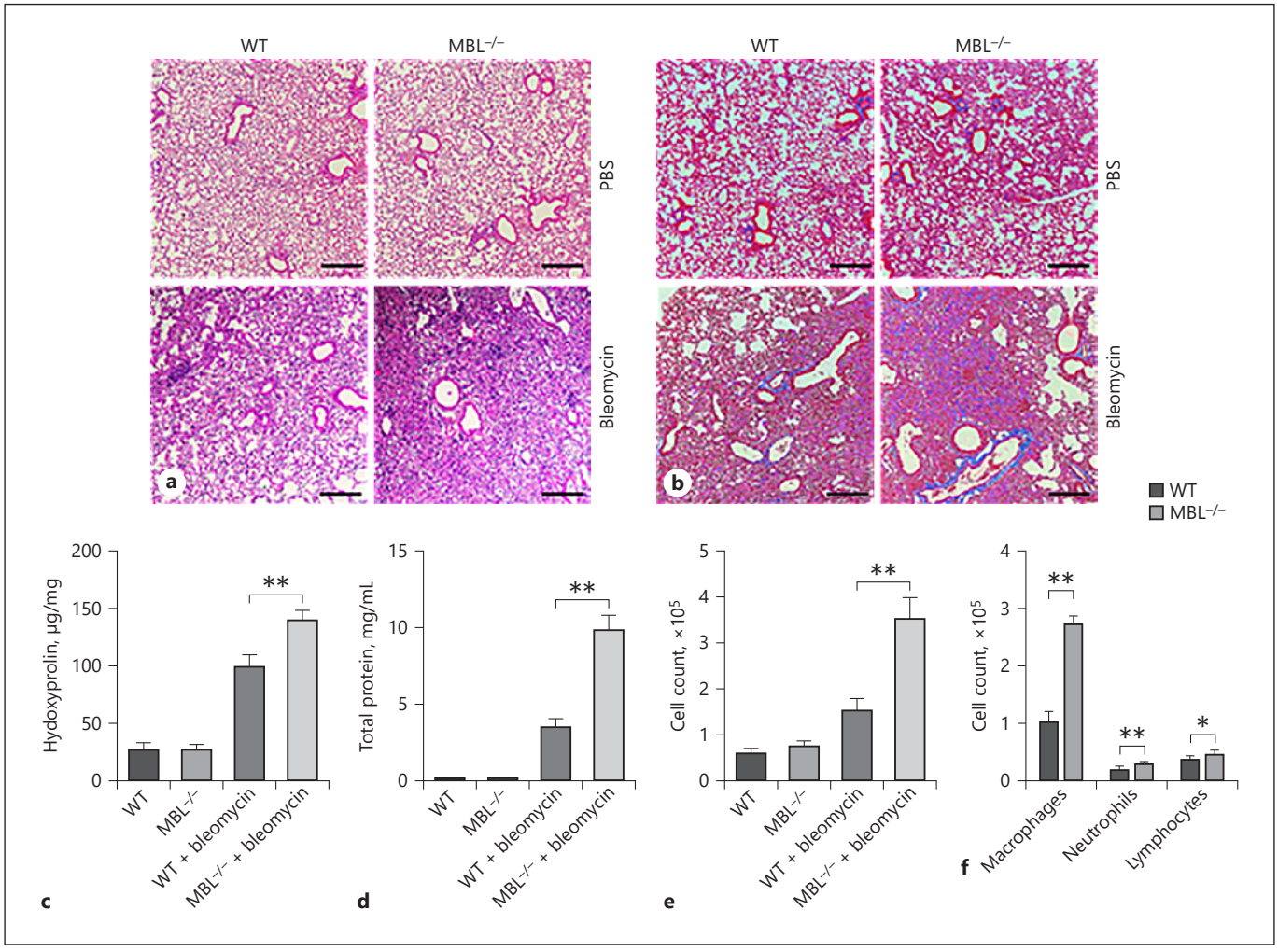

Fig. 1. MBL deficiency aggravated BLM-induced pulmonary fibrosis in mice. **a–e** WT and MBL$^{-/-}$ mice ($n = 5$) were intratracheally injected with 5-mg/kg BLM for 21 days. **a** Histological analysis of mouse lungs was detected by H&E staining. Scale bar, 100 μm. **b** Masson's staining was performed to evaluate pulmonary fibrosis. Scale bar, 100 μm. **c** Hydroxyproline levels in lung tissues were detected. **d** Total protein levels in BALF were determined by BCA analysis. **e** Cell counts in BALF were calculated. **f** Cell differential counts were determined by diff-quick staining. *$p < 0.05$, **$p < 0.01$. The data represent three independent experiments with similar results. One-way ANOVA, followed by Dunnett's post hoc test was used.

clonal antibody, 1:1,000 dilution; Proteintech), GAPDH (60004-1-Ig, mouse anti-human monoclonal antibody, 1:1,000 dilution; Proteintech), and Ub (sc-8017, mouse anti-human monoclonal antibody, 1:1,000 dilution; Santa Cruz Biotechnology).

Statistical Analysis

Statistical analysis was performed by SPSS 12.0 (SPSS, Inc.). The data are presented as the mean ± SD. Unpaired Student's *t* test was used to compare the difference between two groups. Multiple groups comparison was performed by one-way ANOVA, followed by Dunnett's post hoc test. $p < 0.05$ was considered to indicate a statistically significant difference. All experiments were independently repeated in triplicate.

Results

MBL Deficiency Aggravates BLM-Induced Pulmonary Fibrosis

To investigate the effect of MBL on IPF, sex- and age-matched WT or MBL$^{-/-}$ mice were intratracheally injected with BLM for 21 days. Histological analysis showed that lung tissues from MBL$^{-/-}$ mice exhibited aggravated alveolar space obliteration compared with those of WT mice (Fig. 1a). Masson's staining confirmed exacerbated pulmonary fibrosis in MBL$^{-/-}$ mice compared with their WT counterparts (Fig. 1b). Similarly, an increased hy-

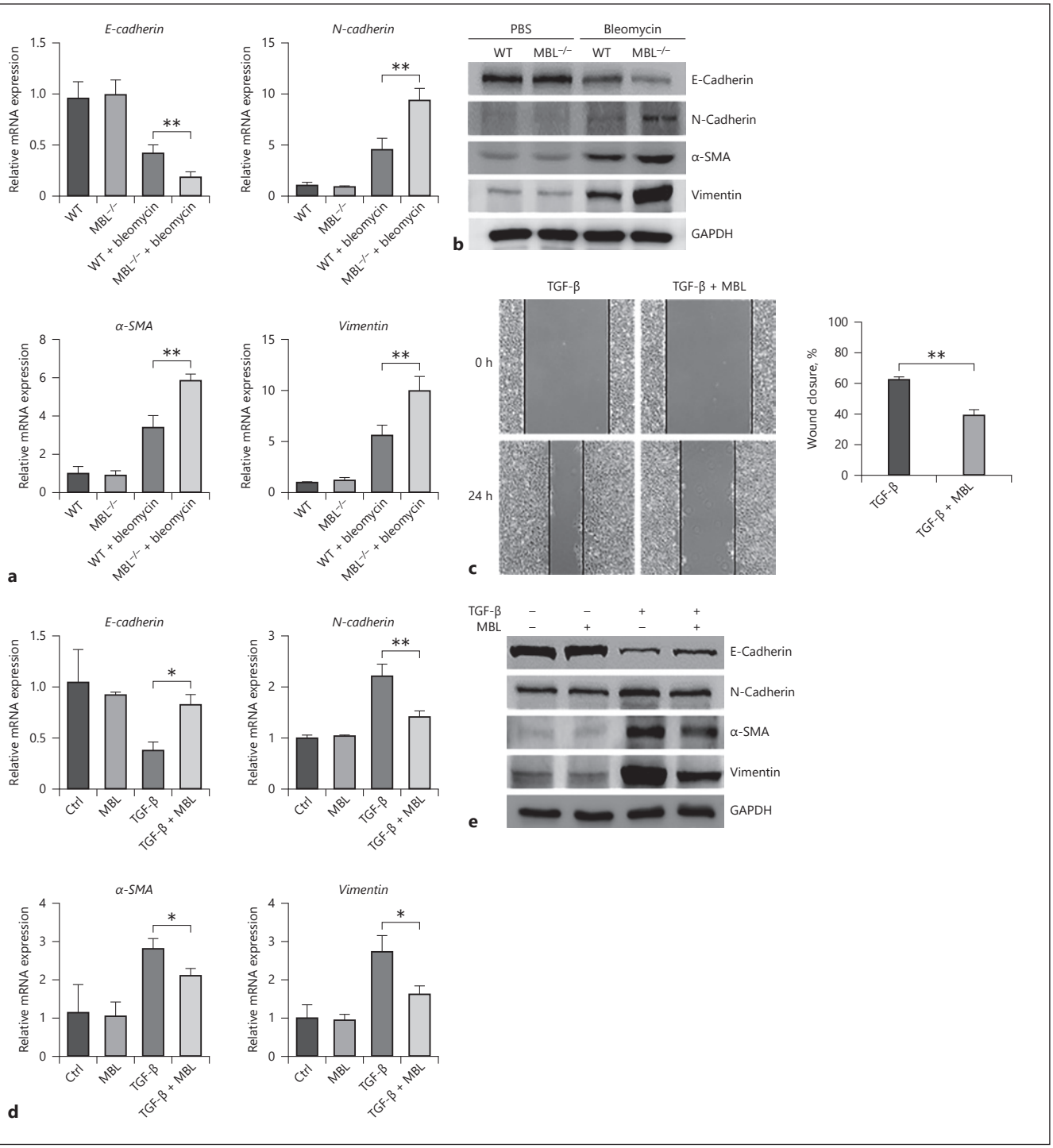

Fig. 2. MBL inhibited EMT phenotype. **a**, **b** 5-mg/kg BLM was intratracheally injected to WT and MBL$^{-/-}$ mice for 21 days. **a** mRNA levels of E-cadherin, N-cadherin, α-SMA, and vimentin were detected by quantitative RT-PCR. **b** E-cadherin, N-cadherin, α-SMA, and vimentin expression were determined by Western blot. **c–e** HBE cells were treated with 10-ng/mL TGF-β in the presence or absence of 10-μg/mL MBL for 24 h. **c** Cell migration was evaluated by wound healing assay. **d** E-cadherin, N-cadherin, α-SMA, and vimentin mRNA expression were assayed by quantitative RT-PCR. **e** Western blot analysis was used to test the expression of E-cadherin, N-cadherin, α-SMA, and vimentin. N.S: not significant, $*p < 0.05$, $**p < 0.01$. The data represent three independent experiments with similar results. One-way ANOVA, followed by Dunnett's post hoc test was used in **a** and **d**. Unpaired Student's *t* test was used in **c**.

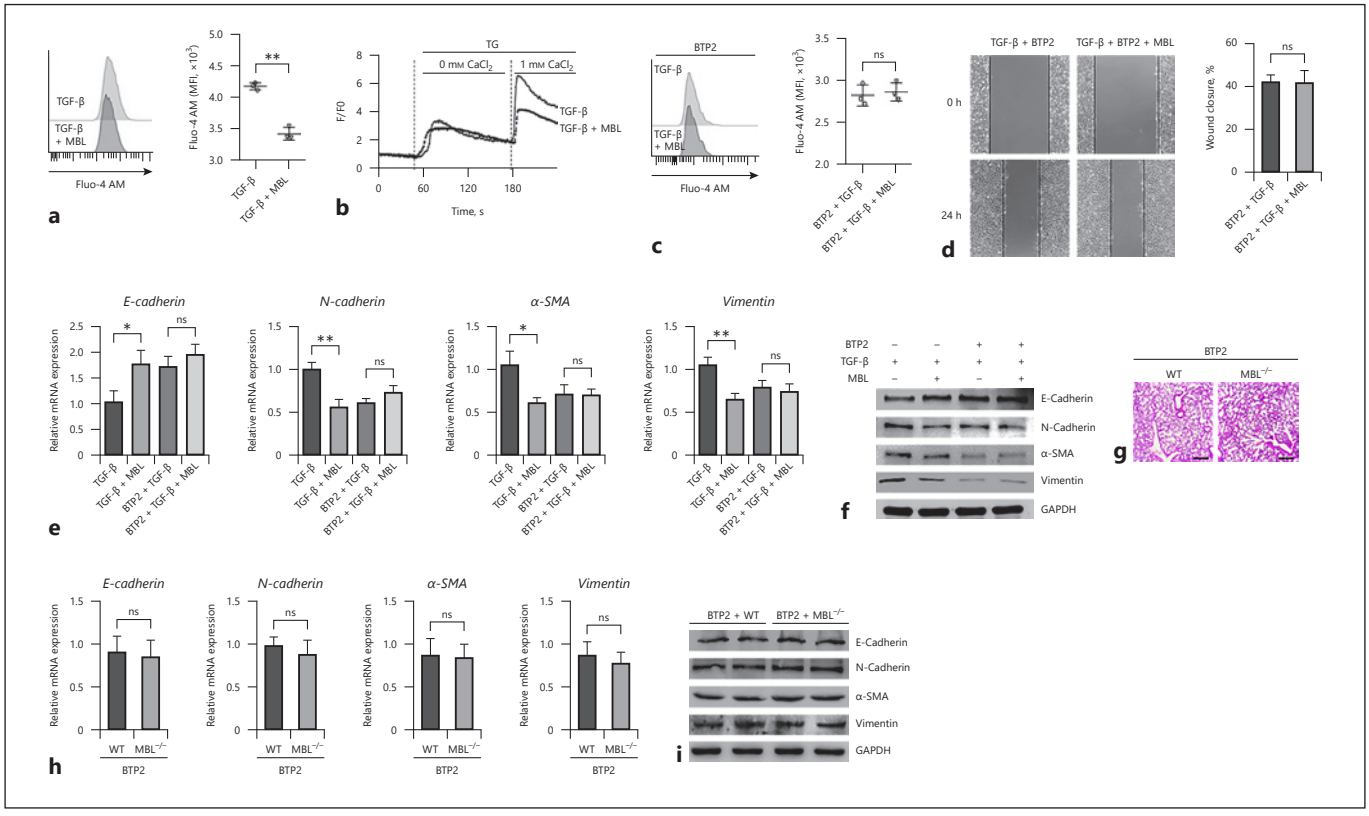

Fig. 3. MBL inhibited EMT phenotype through limited SOCE calcium signaling. **a–f** HBE cells were stimulated with 10-ng/mL TGF-β in the presence or absence of 10-μg/mL MBL for 24 h. In some case, cells were also treated with 3-μM BTP2. **a** FCM analysis was performed to detect cellular calcium. **b** SOCE calcium signaling was assessed by a confocal laser scanning microscope. **c** Cellular calcium was determined by FCM assay. **d** A wound healing assay was used to evaluate cell migration. **e** Quantitative RT-PCR analysis was performed to assay E-cadherin, N-cadherin, α-SMA, and vimentin mRNA expression. **f** E-cadherin, N-cadherin, α-SMA, and vimentin levels were tested by Western blot analysis. **g–i** WT and MBL$^{-/-}$ mice ($n = 5$) were intratracheally injected with 5-mg/kg BLM combined with 10-mg/kg BTP2 for 21 days. **g** Histological analysis of mouse lungs was determined by H&E staining. Scale bar, 100 μm. **h** mRNA levels of E-cadherin, N-cadherin, α-SMA, and vimentin were evaluated by quantitative RT-PCR. **i** E-cadherin, N-cadherin, α-SMA, and vimentin expression were assessed by western blot analysis. ns, not significant, $*p < 0.05$, $**p < 0.01$. The data represent three independent experiments with similar results. Unpaired Student's *t* test was used in **a–d** and **h**. **e** One-way ANOVA, followed by Dunnett's post hoc test was used in **e**.

droxyproline level was detected in the BALF obtained from MBL$^{-/-}$ mice compared with that found in BAF from WT mice (Fig. 1c). Furthermore, increased total protein concentration and cell counts were also found in BALF from MBL$^{-/-}$ mice (Fig. 1d, e). Notably, among the infiltrated immune cells in BALF, macrophages were observed to be the most predominant cell type (Fig. 1f). Together, the results showed that MBL deficiency aggravated BLM-induced pulmonary fibrosis.

MBL Alleviates the EMT Phenotype both in vivo and in vitro

Since EMT is involved in the progression of pulmonary fibrosis [8, 19], the expression of EMT phenotype-related molecules was measured in lung tissues from WT and MBL$^{-/-}$ mice. The results showed both decreased E-cadherin mRNA and protein levels in MBL$^{-/-}$ mice compared with those of their WT counterparts, while increased N-cadherin, α-smooth muscle actin (SMA), and vimentin expression was observed in MBL$^{-/-}$ mice (Fig. 2a, b).

To clarify the effect of MBL on EMT, in vitro studies were performed. Wound healing assays demonstrated reduced migration rates upon MBL treatment (Fig. 2c). Additionally, MBL exposure significantly increased E-cadherin expression at the transcription level. However, N-cadherin, α-SMA, and vimentin expression levels were found to decrease upon MBL exposure (Fig. 2d). Simi-

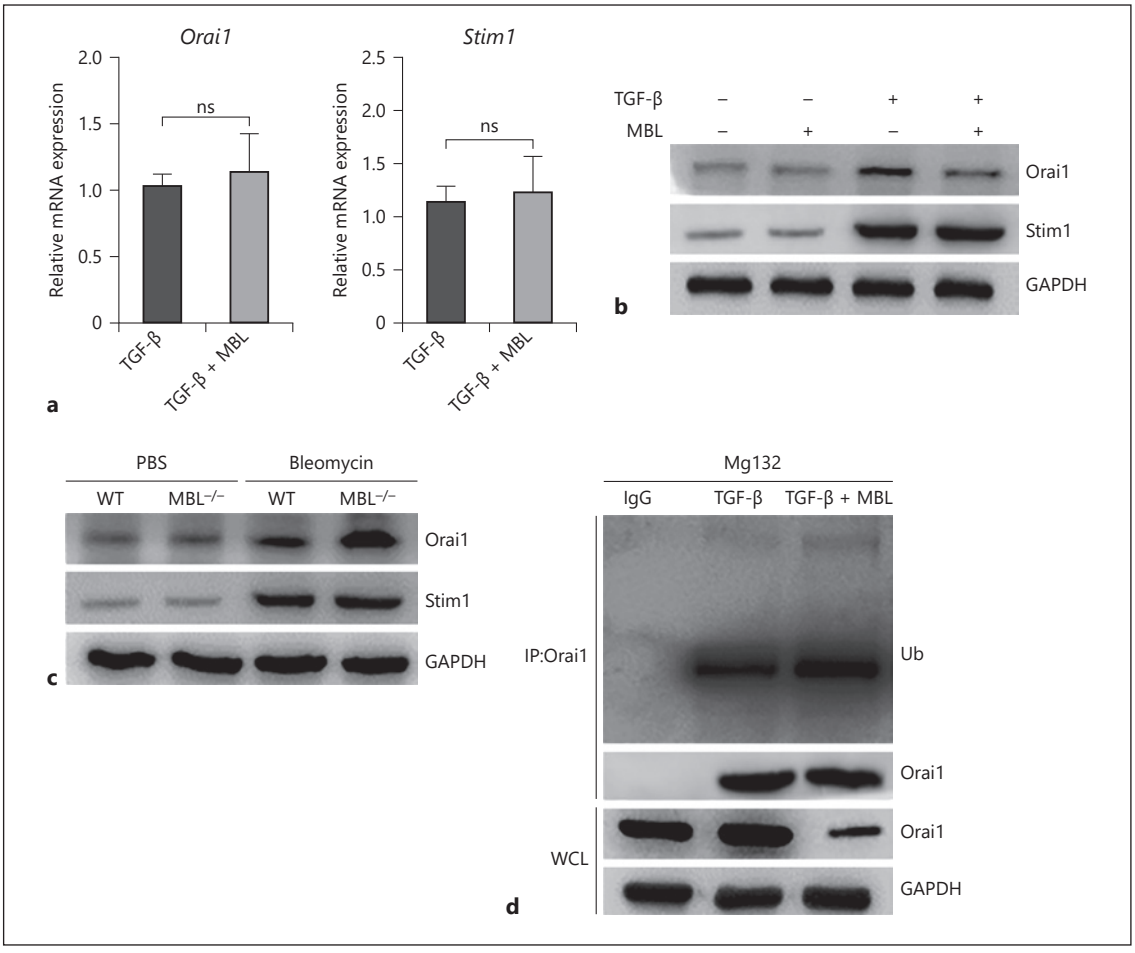

Fig. 4. MBL mediated Orai1 ubiquitination. **a**, **b** HBE cells were incubated with 10-ng/mL TGF-β in the presence or absence of 10-μg/mL MBL for 24 h. **a** mRNA levels of Orai1 and Stim1 were assessed by quantitative RT-PCR. **b** Orai1 and Stim1 expression were determined by Western blot. **c** Orai1 and Stim1 levels in mice lung tissues were detected by Western blot. **d** HBE cells were incubated with 10-ng/mL TGF-β in the presence or absence of 10-μg/mL MBL for 24 h. Cells were treated with 10-μM MG132 4 h before being harvested. The ubiquitination level of Orai1 was detected by immunoprecipitation assay. ns, not significant, $*p < 0.05$, $**p < 0.01$. The data represent three independent experiments with similar results. Unpaired Student's *t* test was used in **a**.

larly, elevated E-cadherin expression along with reduced N-cadherin, α-SMA, and vimentin levels were detected by western blotting (Fig. 2e). Taken together, these data indicated that MBL attenuated the EMT phenotype both in vivo and in vitro.

MBL Regulates the EMT Phenotype through Inhibition of SOCE

It has been reported that calcium signaling is vital for EMT progression [20, 21], and our previous study demonstrated that MBL bound to calreticulin, a calcium buffering chaperone, in T lymphocytes [18]. Thus, the present study explored whether the effect of MBL on EMT involves regulating the calcium channel. First, intracellular calcium levels were evaluated during EMT induction in vitro, and the results showed significantly declined intracellular calcium levels upon MBL treatment (Fig. 3a). Since SOCE is a critical calcium signaling mechanism contributing to EMT [22, 23], the present study next investigated whether MBL influenced SOCE. Notably, SOCE activity was attenuated following MBL exposure (Fig. 3b). To further confirm whether MBL regulated intracellular calcium and EMT through SOCE, BTP2, a SOCE inhibitor, was used. The results showed no significant differences in intracellular calcium levels between cells treated with or without MBL in the presence of BTP2 (Fig. 3c). Similarly, BTP2 abolished the effect of MBL on cell migration during EMT induction conditions (Fig. 3d).

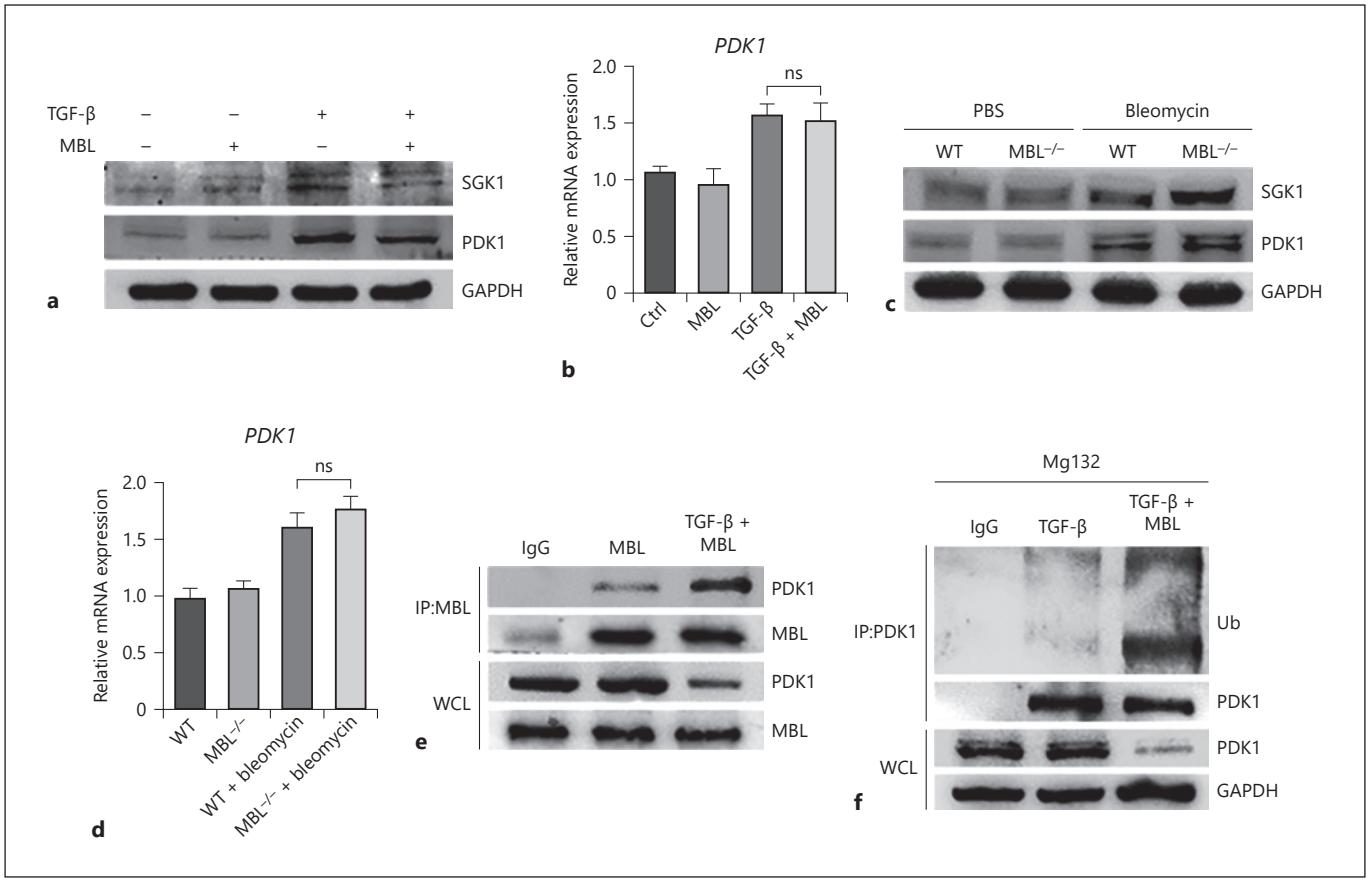

Fig. 5. MBL interacted with PDK1 and contributed to the ubiquitination of PDK1. **a** HBE cells were incubated with 10-ng/mL TGF-β in the presence or absence of 10-μg/mL MBL for 24 h. SGK1 and PDK1 expression were measured by Western blot analysis. **b** PDK1 expression was measured by quantitative RT-PCR. **c** Expression levels of SGK1 and PDK1 in mice lung tissues were determined by Western blot. **d** Expression levels of PDK1 in mice lung tissues were determined by quantitative RT-PCR. **e**, **f** HBE cells were stimulated with 10-ng/mL TGF-β in the presence or absence of 10-μg/mL MBL for 24 h. Cells were treated with 10-μM MG132 4 h before being harvested. **e** Interaction between MBL and PDK1 was detected by immunoprecipitation assay. **f** Ubiquitination level of PDK1 was detected by immunoprecipitation assay. The data represent three independent experiments with similar results.

Similar E-cadherin, N-cadherin, α-SMA, and vimentin expression levels were detected (both at the transcription and translation level) in the TGF-β and TGF-β combined with MBL groups when pretreated with BTP2 (Fig. 3e, f). Next, BTP2 was intratracheally injected into WT or $MBL^{-/-}$ mice in combination with BLM. Unexpectedly, hematoxylin and eosin staining indicated a similar degree of pulmonary fibrosis in WT and $MBL^{-/-}$ mice treated with BTP2 (Fig. 3g). Furthermore, no significant difference in E-cadherin, N-cadherin, α-SMA, or vimentin transcription or translation levels were found in BTP2-injected WT and $MBL^{-/-}$ mice (Fig. 3h, i). Overall, these data suggested that MBL regulated EMT through inhibition of SOCE.

MBL Regulates SOCE through Promoting Orai1 Ubiquitination

Orai1 and stromal interaction molecule 1 (Stim1) are two components that have been identified as essential for SOCE activity [24, 25]. Thus, the current study investigated whether MBL inhibited SOCE through the regulation of Orai1 or Stim1. Unexpectedly, MBL showed no significant effect on Orai1 or Stim1 at the transcription level (Fig. 4a). However, despite MBL exhibited no influence on Stim1 expression at the translational level, Orai1 was found to decline upon MBL treatment (Fig. 4b), which indicated that MBL may regulate the post-translational modification of Orai1. To further confirm these results, lung tissues from WT or

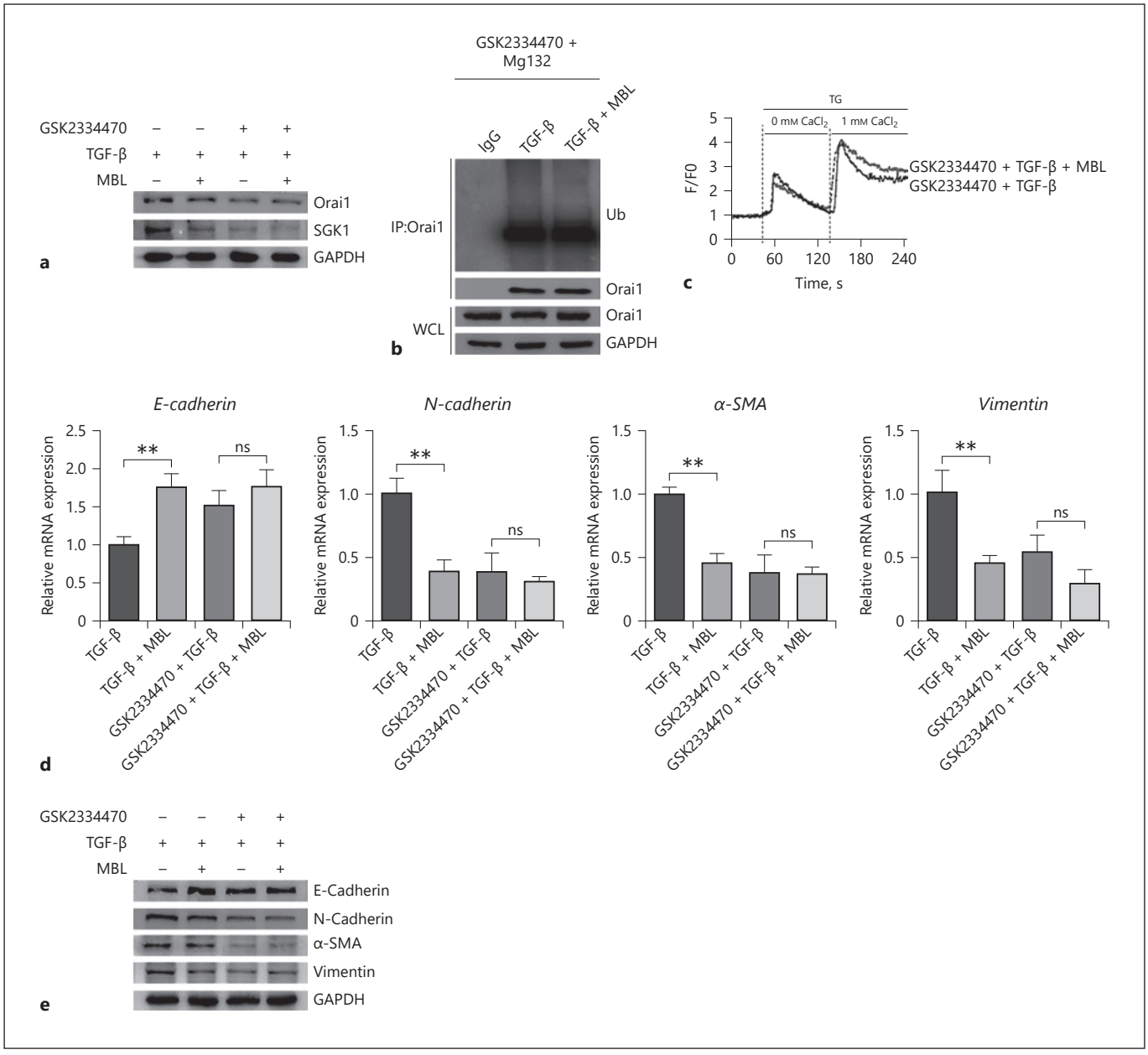

Fig. 6. MBL regulated SOCE activity and EMT phenotype through downregulating PDK1. **a–e** HBE cells were treated with 10-ng/mL TGF-β combined with 5-μM GSK2334470 in the presence or absence of 10-μg/mL MBL for 24 h. **a** Western blot analysis was performed to determine the expression levels of Orai1 and SGK1. **b** The ubiquitination level of Orai1 was tested by immunoprecipitation assay. **c** SOCE calcium signaling was tested by a confocal laser scanning microscope. **d** Expression levels of E-cadherin, N-cadherin, α-SMA, and vimentin were evaluated by quantitative RT-PCR. **e** E-cadherin, N-cadherin, α-SMA, and vimentin levels were assessed by Western blot analysis. N.S: not significant, $*p < 0.05$, $**p < 0.01$. The data represent three independent experiments with similar results. Unpaired Student's *t* test was used in **c**. One-way ANOVA, followed by Dunnett's post hoc test was used in **d**.

$MBL^{-/-}$ mice were evaluated, and increased Orai1 expression was found in $MBL^{-/-}$ mice treated with BLM compared with that of their WT counterparts, while no significant difference of Stim1 was observed between $MBL^{-/-}$ and WT mice (Fig. 4c). It has been reported that Orai1 can be ubiquitinated [26, 27]. Thus, the ubiquitination level of Orai1 was detected, and aggravated Orai1 ubiquitination was observed upon MBL treat-

ment (Fig. 4d). Overall, the data indicated that MBL inhibited SOCE through promoting Orai1 ubiquitination.

MBL Interacts with PDK1 and Promotes PDK1 Ubiquitination

Ubiquitination of Orai1 was reported to be regulated by PDK1-serum/glucocorticoid-regulated kinase 1 (SGK1) signaling [26, 27]. Thus, PDK1 and SGK1 levels were detected. Notably, a decrease in the protein levels of SGK1 and PDK1 were detected under MBL exposure in vitro (Fig. 5a). Similar mRNA levels of SGK1 were detected in cells treated with TGF-β exposed or not to MBL (online suppl. Fig. S1A; see www.karger.com/doi/10.1159/000524693 for all online suppl. material). However, PDK1 mRNA expression exhibited no difference in the presence of MBL (Fig. 5b). Similarly, enhanced expression of SGK1 and PDK1 was found in lung tissues obtained from $MBL^{-/-}$ mice compared with that found in lung tissues obtained from WT mice (Fig. 5c). Additionally, the mRNA expression of SGK1, but not of PDK1, was increased in BLM-treated $MBL^{-/-}$ mice (Fig. 5d; online suppl. Fig. S1B).

Considering that the PDK1 levels are regulated by ubiquitination-mediated proteasome degradation [28, 29], the present study evaluated whether MBL modulated the ubiquitination of PDK1. First, whether MBL directly interacts with PDK1 and SGK1 was investigated. The data showed that MBL could interact with PDK1 (Fig. 5e); however, no detectable interaction between MBL and SGK1 was found (data not shown). Furthermore, enhanced interactions between MBL and PDK1 were found under TGF-β treatment (Fig. 5e). The results showed that MBL treatment promoted the TGF-β-induced ubiquitination of PDK1 (Fig. 5f). Taken together, these data suggested that MBL interacted with PDK1 and was involved in PDK1 ubiquitination.

MBL Regulates SOCE and EMT through PDK1 Signaling

To further confirm whether MBL-modulated SOCE activity depends on PDK1 signaling, a PDK1 inhibitor, GSK2334470, was employed. The results showed comparable levels of Orai1 and SGK1 in TGF-β-treated cells with or without MBL treatment when PDK1 was inhibited (Fig. 6a). GSK2334470 treatment abolished the regulatory effect of MBL on Orai1 ubiquitination in TGF-β-treated cells (Fig. 6b). No significant difference in TGF-β-induced SOCE activity was observed in TGF-β and TGF-β plus MBL-treated cells upon pre-exposure to GSK2334470 (Fig. 6c). Next, the current study investigated whether PDK1 inhibition influences the effect of MBL on the EMT process. The results showed similar expression of E-cadherin, N-cadherin, α-SMA, and vimentin in TGF-β and TGF-β plus MBL-treated cells in the presence of GSK2334470 both at the transcriptional and translational level (Fig. 6d, e). Taken together, the data indicated that MBL regulated SOCE activity and the EMT process through PDK1 signaling.

Discussion

MBL is a hepatocyte-derived soluble calcium-dependent complement molecule, which modulates inflammation during infection and tissue damage. The present study demonstrated that MBL is a pivotal mediator to protect against BLM-induced pulmonary fibrosis in mice. Upon BLM challenge, $MBL^{-/-}$ mice exhibited exacerbated lung fibrosis and aggravated EMT process. This was manifested by alleviation of the TGF-β-induced EMT in MBL-treated AECs. MBL affected SOCE and decreased the intracellular calcium levels in AECs subjected to TGF-β exposure. BTP2, a novel inhibitor of SOCE, abolished the MBL-mediated downregulation of the TGF-β-induced EMT process. In addition, inhibition of SOCE attenuated lung fibrosis after BLM administration and abolished the difference in lung pathology between BLM-challenged WT and $MBL^{-/-}$ mice. Furthermore, MBL modulated the SOCE machinery via interaction with PDK1. These results indicated that MBL is pivotal for intracellular calcium homeostasis that contributes to the EMT process during BLM-induced pulmonary fibrosis.

Increasing evidence has shown that, during pulmonary fibrogenesis, EMT acts as a primary pool of pathogenic myofibroblasts and leads to the formation of fibroblastic foci in mice and humans [25, 27–29]. Prevention of EMT significantly attenuated BLM-induced pulmonary fibrosis in mice [30]. Notably, exclusive expression of β-galactosidase in mouse lung epithelial cells induced the expression of mesenchymal markers after TGF-β production [4]. It is crucial to distinguish between factors that promote EMT and those that induce the death of epithelial cells or enhance the proliferation of mesenchymal cells. The present study provided evidence that MBL limited the EMT phenotype in AECs. It should be mentioned that all myofibroblasts express α-SMA, which has been found to be upregulated in lung fibrosis. TGF-β stimulation significantly reduced E-cadherin expression and increased N-cadherin, α-SMA and vimentin expression. The present study revealed that MBL limited the TGF-β-induced expression of EMT-related

molecules in AECs. Therefore, it was speculated that the modulation of EMT by MBL may be clinically relevant. The investigation of the underlying molecular mechanism will help to understand the pathophysiological role of MBL in EMT-associated diseases.

Calcium is an important multifunctional secondary messenger that modulates a diverse range of physiological and pathological processes. The cytosolic calcium level is strictly controlled by a complex calcium signaling system that includes calcium channels, pumps, and exchangers. In nonexcitable cells, SOCE is the predominant calcium entry mechanism. Increased SOCE activity may result in EMT and may promote cell migration and invasion [31]. When Stim1 expression was inhibited with small hairpin RNA, TGFβ-induced EMT was abolished, which indicated that SOCE was required for TGFβ-mediated EMT [32]. Orai1 is a key calcium channel pore-forming protein, which is located on the plasma membrane and functions as a pore-forming unit to initiate calcium influx across the plasma membrane. It should be noted that Orai1-mediated SOCE has been considered to exert a crucial effect on the development of various cancer types. Kang et al. [23] found that, in colorectal cancer cells, Orai1 promoted TGF-β-induced EMT by inducing calcium entry and calpain activity. The results of the present study suggested that MBL promoted the ubiquitination and subsequent degradation of Orai1. However, a direct interaction between MBL and Orai1 was not observed. It is noteworthy that Orai1 is a ubiquitous protein that forms the calcium release-activated channel [33]. Several studies have determined that Orai1 directly interacts with ubiquitin ligases, thereby modulating its ubiquitination and expression level [34–36].

Both Orai1 and Stim1 expression have been reported to be stimulated by the NF-κB signaling pathway, which interacts with the corresponding promoter regions of the genes encoding Stim1 and Orai1 [34]. SGK1 is one of the protein serine/threonine kinases stimulated by growth factors via the PI3K signaling pathway [37]. Decreased Orai1 protein levels in *sgk1*$^{-/-}$ platelets could be due to limited Orai1 transcription or increased degradation of Orai1 protein [38]. Indeed, SGK1-mediated regulation of SOCE appears to be critically important for calcium transport. Lang et al. [35] determined that SGK1 upregulates, while AMPK presumably downregulates, NF-κB and thus the de novo synthesis of Orai1 and Stim1 proteins. The present study showed that MBL significantly inhibited the expression of Orai1 and Stim1 in AECs upon TGF-β stimulation. It should be mentioned that MBL treatment could inhibit LPS-induced NF-κB DNA binding and translocation in monocytes [11]. Therefore, it is possible that the NF-κB signaling activation may be involved in the MBL-mediated modulation of Orai1 and Stim1 expression. SGK1 has been reported to regulate diverse ion channels by binding to ubiquitin ligases [26, 27, 39]. PDK1 is activated by TGF-β and induces the EMT process and promotes proliferation and invasion in human glioblastoma [40]. A previous study demonstrated that SGK1 was activated by PDK1, which sustained AKT-independent mTORC1 activation [41]. The present results demonstrated that MBL suppressed the TGF-β-induced expression of PDK1 and SGK1 both in vivo and in vitro. Notably, MBL directly interacted with PDK1 and promoted its ubiquitination upon TGF-β stimulation. It was also shown that blocking PDK1 function abrogated MBL-modulated Orai1 expression and calcium transport, suggesting that the PDK1-SGK1 axis accounts for the MBL-mediated regulation of SOCE activity and subsequent EMT process.

Overall, the results of the present study indicated that the protective role of MBL in pulmonary fibrosis may be associated with its regulation of calcium influx. These findings provide novel insights into the pathogenesis of pulmonary fibrosis. The present study elucidated an unknown feature of MBL function in modulating SOCE activity. MBL could be considered a potential therapeutic target for IPF. Further studies on human samples or disease models are required to identify the practicability and potential therapeutic benefit of targeting MBL in fibrotic diseases in the future.

Statement of Ethics

All animal experiments in this study were approved by the Welfare and Ethical Committee for Experimental Animal Care of Southern Medical University (approval No. L2016014).

Conflict of Interest Statement

The authors have no conflicts of interest to declare.

Funding Source

This work was supported in part by the National Natural Science Foundation of China (Grant No. 82171745, 82071781, 81971550, and 81873872), Science and Technology Planning Project of Guangzhou (Grant No. 202002030160), and innovation team of chronic kidney disease with integrated traditional Chinese and Western medicine (Grant No. 2019KCXTD014).

Author Contributions

Y.L., Z.C., and D.Z. designed the research. Y.L., X.X., J.L., Q.X., J.Z., P.W., and X.L. conceived the experiments and performed the data analysis. Y.L., X.X., Y.C., and Z.C. analyzed the data. Z.L., J.Z., J.C., and D.Z. wrote and revised the manuscript with input from all coauthors.

Data Availability Statement

The data used to support the findings of this study are included within the article.

References

1 Richeldi L, Collard HR, Jones MG. Idiopathic pulmonary fibrosis. Lancet. 2017 May 13; 389(10082):1941–52.
2 Chen Q, Liu Y. Heterogeneous groups of alveolar type II cells in lung homeostasis and repair. Am J Physiol Cell Physiol. 2020 Dec; 319(6):C991–6.
3 Parimon T, Yao C, Stripp BR, Noble PW, Chen P. Alveolar epithelial type II cells as drivers of lung fibrosis in idiopathic pulmonary fibrosis. Int J Mol Sci. 2020 Apr;21(7): 2269.
4 Kalluri R, Neilson EG. Epithelial-mesenchymal transition and its implications for fibrosis. J Clin Invest. 2003 Dec;112(12):1776–84.
5 Kalluri R, Weinberg RA. The basics of epithelial-mesenchymal transition. J Clin Invest. 2009 Jun;119(6):1420–8.
6 Bartis D, Mise N, Mahida RY, Eickelberg O, Thickett DR. Epithelial-mesenchymal transition in lung development and disease: does it exist and is it important? Thorax. 2014 Aug; 69(8):760–5.
7 Hill C, Jones MG, Davies DE, Wang Y. Epithelial-mesenchymal transition contributes to pulmonary fibrosis via aberrant epithelial/fibroblastic cross-talk. J Lung Health Dis. 2019 Apr 2;3(2):31–5.
8 Namba T, Tanaka KI, Ito Y, Hoshino T, Matoyama M, Yamakawa N, et al. Induction of EMT-like phenotypes by an active metabolite of leflunomide and its contribution to pulmonary fibrosis. Cell Death Differ. 2010 Dec; 17(12):1882–95.
9 Willis BC, Borok Z. TGF-beta-induced EMT: mechanisms and implications for fibrotic lung disease. Am J Physiol Lung Cell Mol Physiol. 2007 Sep;293(3):L525–34.
10 Gadjeva M, Takahashi K, Thiel S. Mannan-binding lectin--a soluble pattern recognition molecule. Mol Immunol. 2004 Jun;41(2–3): 113–21.
11 Wang M, Chen Y, Zhang Y, Zhang L, Lu X, Chen Z. Mannan-binding lectin directly interacts with Toll-like receptor 4 and suppresses lipopolysaccharide-induced inflammatory cytokine secretion from THP-1 cells. Cell Mol Immunol. 2011 May;8(3):265–75.
12 Eisen DP. Mannose-binding lectin deficiency and respiratory tract infection. J Innate Immun. 2010;2(2):114–22.
13 Dicker AJ, Crichton ML, Cassidy AJ, Brady G, Hapca A, Tavendale R, et al. Genetic mannose binding lectin deficiency is associated with airway microbiota diversity and reduced exacerbation frequency in COPD. Thorax. 2018 Jun;73(6):510–8.
14 Hodge S, Matthews G, Dean MM, Ahern J, Djukic M, Hodge G, et al. Therapeutic role for mannose-binding lectin in cigarette smoke-induced lung inflammation? Evidence from a murine model. Am J Respir Cell Mol Biol. 2010 Feb;42(2):235–42.
15 Malaquias MAS, Gadotti AC, Motta-Junior JDS, Martins APC, Azevedo MLV, Benevides APK, et al. The role of the lectin pathway of the complement system in SARS-CoV-2 lung injury. Transl Res. 2021 May;231:55–63.
16 Kolb P, Upagupta C, Vierhout M, Ayaub E, Bellaye PS, Gauldie J, et al. The importance of interventional timing in the bleomycin model of pulmonary fibrosis. Eur Respir J. 2020 Jun; 55(6):1901105.
17 Takemasa A, Ishii Y, Fukuda T. A neutrophil elastase inhibitor prevents bleomycin-induced pulmonary fibrosis in mice. Eur Respir J. 2012 Dec;40(6):1475–82.
18 Zhao N, Wu J, Xiong S, Zhang L, Lu X, Chen S, et al. Mannan-binding lectin, a serum collectin, suppresses T-cell proliferation via direct interaction with cell surface calreticulin and inhibition of proximal T-cell receptor signaling. FASEB J. 2017 Jun;31(6):2405–17.
19 Kim KK, Wei Y, Szekeres C, Kugler MC, Wolters PJ, Hill ML, et al. Epithelial cell alpha3beta1 integrin links beta-catenin and Smad signaling to promote myofibroblast formation and pulmonary fibrosis. J Clin Invest. 2009 Jan;119(1):213–24.
20 Davis FM, Azimi I, Faville RA, Peters AA, Jalink K, Putney JW Jr, et al. Induction of epithelial-mesenchymal transition (EMT) in breast cancer cells is calcium signal dependent. Oncogene. 2014 May 1;33(18):2307–16.
21 Liu L, Wu N, Wang Y, Zhang X, Xia B, Tang J, et al. TRPM7 promotes the epithelial-mesenchymal transition in ovarian cancer through the calcium-related PI3K / AKT oncogenic signaling. J Exp Clin Cancer Res. 2019 Feb 28;38(1):106.
22 Kang Q, Peng X, Li X, Hu D, Wen G, Wei Z, et al. Calcium channel protein ORAI1 mediates TGF-beta induced epithelial-to-mesenchymal transition in colorectal cancer cells. Front Oncol. 2021;11:649476.
23 Wei J, Deng Y, Ye J, Luo Y, Weng J, He Q, et al. Store-operated Ca(2+) entry as a key oncogenic Ca(2+) signaling driving tumor invasion-metastasis cascade and its translational potential. Cancer Lett. 2021 Sep 28;516:64–72.
24 Feske S. ORAI1 and STIM1 deficiency in human and mice: roles of store-operated Ca2+ entry in the immune system and beyond. Immunol Rev. 2009 Sep;231(1):189–209.
25 Lian J, Cuk M, Kahlfuss S, Kozhaya L, Vaeth M, Rieux-Laucat F, et al. ORAI1 mutations abolishing store-operated Ca(2+) entry cause anhidrotic ectodermal dysplasia with immunodeficiency. J Allergy Clin Immunol. 2018 Oct;142(4):1297–310 e11.
26 Shumilina E, Zemtsova IM, Heise N, Schmid E, Eichenmuller M, Tyan L, et al. Phosphoinositide-dependent kinase PDK1 in the regulation of Ca2+ entry into mast cells. Cell Physiol Biochem. 2010;26(4–5):699–706.
27 Eylenstein A, Gehring EM, Heise N, Shumilina E, Schmidt S, Szteyn K, et al. Stimulation of Ca2+-channel Orai1/STIM1 by serum- and glucocorticoid-inducible kinase 1 (SGK1). FASEB J. 2011 Jun;25(6):2012–21.
28 Fujita N, Sato S, Ishida A, Tsuruo T. Involvement of Hsp90 in signaling and stability of 3-phosphoinositide-dependent kinase-1. J Biol Chem. 2002 Mar 22;277(12): 10346–53.
29 Wei Q, Xia Y. Roles of 3-phosphoinositide-dependent kinase 1 in the regulation of endothelial nitric-oxide synthase phosphorylation and function by heat shock protein 90. J Biol Chem. 2005 May 6;280(18):18081–6.
30 Borok Z. Role for alpha3 integrin in EMT and pulmonary fibrosis. J Clin Invest. 2009 Jan; 119(1):7–10.
31 Mo P, Yang S. The store-operated calcium channels in cancer metastasis: from cell migration, invasion to metastatic colonization. Front Biosci. 2018 Jan 1;23:1241–56.
32 Hu J, Qin K, Zhang Y, Gong J, Li N, Lv D, et al. Downregulation of transcription factor Oct4 induces an epithelial-to-mesenchymal transition via enhancement of Ca2+ influx in breast cancer cells. Biochem Biophys Res Commun. 2011 Aug 12;411(4):786–91.
33 Moccia F, Zuccolo E, Soda T, Tanzi F, Guerra G, Mapelli L, et al. Stim and Orai proteins in neuronal Ca(2+) signaling and excitability. Front Cell Neurosci. 2015;9:153.
34 Lang F, Eylenstein A, Shumilina E. Regulation of Orai1/STIM1 by the kinases SGK1 and AMPK. Cell Calcium. 2012 Nov;52(5):347–54.

35 Lee JE, Jeon IS, Han NE, Song HJ, Kim EG, Choi JW, et al. Ubiquilin 1 interacts with Orai1 to regulate calcium mobilization. Mol Cells. 2013 Jan;35(1):41–6.
36 Moon H, Min C, Kim G, Kim D, Kim K, Lee SA, et al. Crbn modulates calcium influx by regulating Orai1 during efferocytosis. Nat Commun. 2020 Oct 30;11(1):5489.
37 Di Cristofano A SGK1: the dark side of PI3K signaling. Curr Top Dev Biol. 2017;123:49.
38 Borst O, Schmidt EM, Munzer P, Schonberger T, Towhid ST, Elvers M, et al. The serum- and glucocorticoid-inducible kinase 1 (SGK1) influences platelet calcium signaling and function by regulation of Orai1 expression in megakaryocytes. Blood. 2012 Jan 5;119(1):251–61.
39 Lang F, Shumilina E. Regulation of ion channels by the serum- and glucocorticoid-inducible kinase SGK1. Faseb J. 2013 Jan;27(1):3–12.
40 Luo D, Xu X, Li J, Chen C, Chen W, Wang F, et al. The PDK1/cJun pathway activated by TGFbeta induces EMT and promotes proliferation and invasion in human glioblastoma. Int J Oncol. 2018 Nov;53(5):2067–80.
41 Castel P, Ellis H, Bago R, Toska E, Razavi P, Carmona FJ, et al. PDK1-SGK1 signaling sustains AKT-independent mTORC1 activation and confers resistance to PI3K alpha inhibition. Cancer Cell. 2016 Aug 8;30(2):229–42.